



Geophysical Research Letters



RESEARCH LETTER

10.1029/2023GL107119

Key Points:

- The La Niña's regulation of Indian Ocean Oscillation (IOD) mainly depends on the La Niña longitudinal position
- The westward-displaced La Niña events produce significant Walker Circulation anomalies, triggering robust negative IOD event
- The importance of La Niña longitudinal position on the IOD's response can be evidenced by the targeted pacemaker experiments

Supporting Information:

Supporting Information may be found in the online version of this article.

Correspondence to:

W. Zhang, zhangwj@nuist.edu.cn

Citation:

Zhang, T., Zhang, W., Jiang, F., & Jin, F.-F. (2024). La Niña's teleconnection to the Indian Ocean Dipole controlled by its longitudinal position. *Geophysical Research Letters*, *51*, e2023GL107119. https://doi.org/10.1029/2023GL107119

Received 13 NOV 2023 Accepted 20 JAN 2024

© 2024. The Authors.

This is an open access article under the terms of the Creative Commons

Attribution-NonCommercial-NoDerivs

License, which permits use and distribution in any medium, provided the original work is properly cited, the use is non-commercial and no modifications or adaptations are made.

La Niña's Teleconnection to the Indian Ocean Dipole Controlled by Its Longitudinal Position

Teng Zhang¹, Wenjun Zhang¹, Feng Jiang^{1,2}, and Fei-Fei Jin³

¹CIC-FEMD/ILCEC, Key Laboratory of Meteorological Disaster of Ministry of Education (KLME), Nanjing University of Information Science and Technology, Nanjing, China, ²Lamont-Doherty Earth Observatory, Columbia University, Palisades, NY, USA, ³Department of Atmospheric Sciences, School of Ocean and Earth Science and Technology (SOEST), University of Hawai'i at Mānoa, Honolulu, HI, USA

Abstract While the prominent influence of El Niño-Southern Oscillation (ENSO) on the Indian Ocean Oscillation (IOD) is widely recognized, intricate relationships between them are often invoked that introduce challenges into seasonal predictions. Previous studies have shown that different flavors of El Niño exhibit distinct associations with the IOD. In this study, we demonstrate that La Niña's teleconnection to the IOD is primarily controlled by its longitudinal position. Westward-displaced La Niña events tend to produce stronger negative convection anomalies in the central Pacific and more pronounced Walk Circulation anomalies, thereby triggering strong negative IOD events. In contrast, eastward-displaced La Niña events are usually accompanied by feeble convection response due to the excessively cold conditions in the cold tongue, yielding insignificant IOD response. The pivotal role of La Niña's longitudinal position on the IOD's response is realistically reproduced by targeted pacemaker experiments, providing new insights into inter-basin climate connections.

Plain Language Summary The tropical Indian Ocean usually witnesses a dipolar pattern of sea surface temperature (SST) anomalies, which is commonly referred to as the Indian Ocean Dipole (IOD). The IOD phenomenon has received much attention due to its profound global impacts, yet its seasonal prediction remains a large challenge for the climate community. The year-to-year variability of IOD has usually been linked to the El Niño–Southern Oscillation (ENSO), the predominant interannual climate variability in the tropical Pacific. The relationship between El Niño (i.e., warm phase of ENSO) and the intensity of IOD has been demonstrated in previous studies, which is shown to be dependent on the different El Niño flavors. In this study, we show that the longitudinal position of negative SST anomalies during La Niña events (i.e., cold phase of ENSO) in shaping their connection with IOD. Different from westward-displaced La Niña events that can drive robust negative IOD events, eastward-displaced La Niña events do not yield significant IOD anomalies due to the excessively cold conditions prevalent in the eastern Pacific cold tongue region. We highlight the importance of La Niña's longitudinal position in its teleconnection to other ocean basins and the associated regional climate anomalies.

1. Introduction

A dipole pattern of sea surface temperature (SST) anomalies usually emerges in the tropical Indian Ocean (IO), which is commonly referred to as the Indian Ocean Dipole (IOD) (Saji et al., 1999; Webster et al., 1999). A positive IOD event is characterized by cooling SST along the Java-Sumatra coast and accompanied by simultaneous warming SST in the western tropical IO. The typical IOD develops in boreal summer, matures in autumn, and rapidly decays in the following seasons. The IOD has aroused widespread concerns in the scientific community due to its far-reaching global effects, affecting regions such as East Africa (Saji et al., 1999), the Asian-Australian monsoon zone (e.g., Ashok et al., 2001; Cai & Cowan, 2008; Zhang et al., 2021).

The IOD events are frequently observed to co-occur with the El Niño-Southern Oscillation (ENSO) conditions in the tropical Pacific. Specifically, positive IOD events are typically accompanied by El Niño events, while negative IOD events are commonly linked to La Niña events (e.g., Allan et al., 2001; Annamalai et al., 2003; Baquero-Bernal et al., 2002; Xie et al., 2002). As the predominant interannual climate variability, the ENSO can drive climate anomalies that extend beyond the tropical Pacific, affecting global climate through atmospheric and oceanic teleconnections (e.g., Alexander et al., 2002; Klein et al., 1999; Lau & Nath, 2003). ENSO has long been considered as an important external forcing for the IOD SST variability (Fan et al., 2017; Li et al., 2003; Scott et al., 2009; Stuecker et al., 2017; Wang et al., 2019), while some earlier studies argued that the IOD might be an

ZHANG ET AL. 1 of 10

internal mode (Saji et al., 1999; Webster et al., 1999). Despite that the exact nature of the IOD dynamics remains open to debate, ENSO serves as the primary predictability source of IOD on the seasonal to interannual timescales (e.g., Liu et al., 2022; Zhao et al., 2020).

Over the last two decades, a new type of El Niño has become frequent in the central tropical Pacific (referred to as central Pacific El Niño, CP El Niño), which is distinctly different from the traditional El Niño type with its SST anomaly center located in the eastern tropical Pacific (known as eastern Pacific El Niño, EP El Niño) (e.g., Ashok et al., 2007; Kao & Yu, 2009; Kug et al., 2009; Larkin & Harrison, 2005). These two flavors of El Niño exhibit different associations with IOD, as highlighted in the prior research (Zhang, Wang, Jin, et al., 2015; Zhang, Wang, Xiang, et al., 2015). EP El Niño events display a robust relationship with the IOD dependent on their intensity, whereas the connection between CP El Niño events and the IOD is primarily determined by the longitudinal position of the El Niño-related positive SST anomalies rather than the magnitude.

In contrast to the ENSO warm phase, the SST anomalies during the cold phase (i.e., La Niña) are typically displaced westward, considering the outcropping thermocline nonlinearity due to the shallow background thermocline in the Pacific cold tongue region. At present, the classification of La Niña into different flavors and identification of key factors governing its climate impacts remain subjects of debate (e.g., Cai & Cowan, 2009; Kug & Ham, 2011; Ren & Jin, 2011; Zhang, Wang, Jin, et al., 2015; Zhang, Wang, Xiang, et al., 2015). In the study, we investigate the complicated connection of La Niña with the IOD and we found that the teleconnection of La Niña to IOD is primarily determined by the longitudinal positioning of SST anomalies.

2. Methods

Our analyses cover the period of 1960–2022 for all data sets, except for the data set from GODAS only available from 1980 to 2022. All data sets are linearly detrended to avoid the potential impact of global warming. We conducted all statistical significance tests using the two-tailed Student's *t*-test.

We further examined the outputs from ensembles of tropical Pacific Pacemaker experiments (comprising 10 members) using the National Center for Atmospheric Research Community Earth System Model version 2 (NCAR CESM2) (Danabasoglu et al., 2020), evidencing the main conclusion based on the observation. In these simulations, the SST anomalies related to ENSO in the central and eastern Pacific were fully nudged toward observations within the 15°S–15°N latitude range during 1880–2019. The region outside the nudging area is allowed to evolve freely. To focus on the impacts of tropical Pacific ENSO and eliminate the possible influence from the internal process in the tropical IO, our analyses were built upon the ensemble mean in the period (1960–2019).

ENSO intensity is measured using the Niño3.4 index, computed as the average SST anomalies within the 5°S–5° N and 120°–170°W region. The intensity of IOD is described as the dipole mode index (DMI), representing the SST anomaly zonal gradient between the western equatorial (10°S–10°N and 50°–70°E) and southeastern equatorial Indian Ocean (10°S–0° and 90°–110°E) (Saji et al., 1999). The La Niña events are chosen when the 3-month running mean Niño3.4 index falls below -0.3°C in summer (June–July–August) and -0.5°C in autumn (September–October–November). We here identify 18 La Niña events (1964, 1970, 1971, 1973, 1974, 1975, 1985, 1988, 1998, 1999, 2000, 2007, 2010, 2011, 2016, 2020, 2021, 2022). For the CESM2 pacemaker experiment, 15 La Niña events are analyzed due to the available simulation before 2019.

To understand the relative role of dynamic and thermodynamic processes in regulating the IOD development, the ocean mixed layer heat budget is investigated (e.g., Jin et al., 2003), which can be expressed as:

$$\begin{split} \frac{\partial T'}{\partial t} &= - \left(u' \frac{\partial \overline{T}}{\partial x} + \overline{u} \frac{\partial T'}{\partial x} + u' \frac{\partial T'}{\partial x} \right) - \left(v' \frac{\partial \overline{T}}{\partial y} + \overline{v} \frac{\partial T'}{\partial y} + v' \frac{\partial T'}{\partial y} \right) \\ &- \left(w' \frac{\partial \overline{T}}{\partial z} + \overline{w} \frac{\partial T'}{\partial z} + w' \frac{\partial T'}{\partial z} \right) + \frac{Q'_{\text{net}}}{\rho c_p H} + R \end{split}$$

In the given equations, the overbar and prime denote the climatological mean and corresponding anomaly, respectively. T denotes potential temperature; u and v represent zonal and meridional ocean current velocities, respectively; and w indicates the vertical ocean current velocity. The term Q_{net} represents the net surface heat flux, which includes surface shortwave radiation, surface longwave radiation, latent heat fluxes, and sensible heat

ZHANG ET AL. 2 of 10

1944807, 2024, 3, Downloaded from https://agupubs.onlinelibrary.wiley.com/doi/10.1029/2023GL107119, Wiley Online Library on [18/042024]. See the Terms and Conditions (https://onlinelibrary.wiley.com/terms-and-conditions) on Wiley Online Library for rules of use; OA articles are governed by the applicable Creative C.

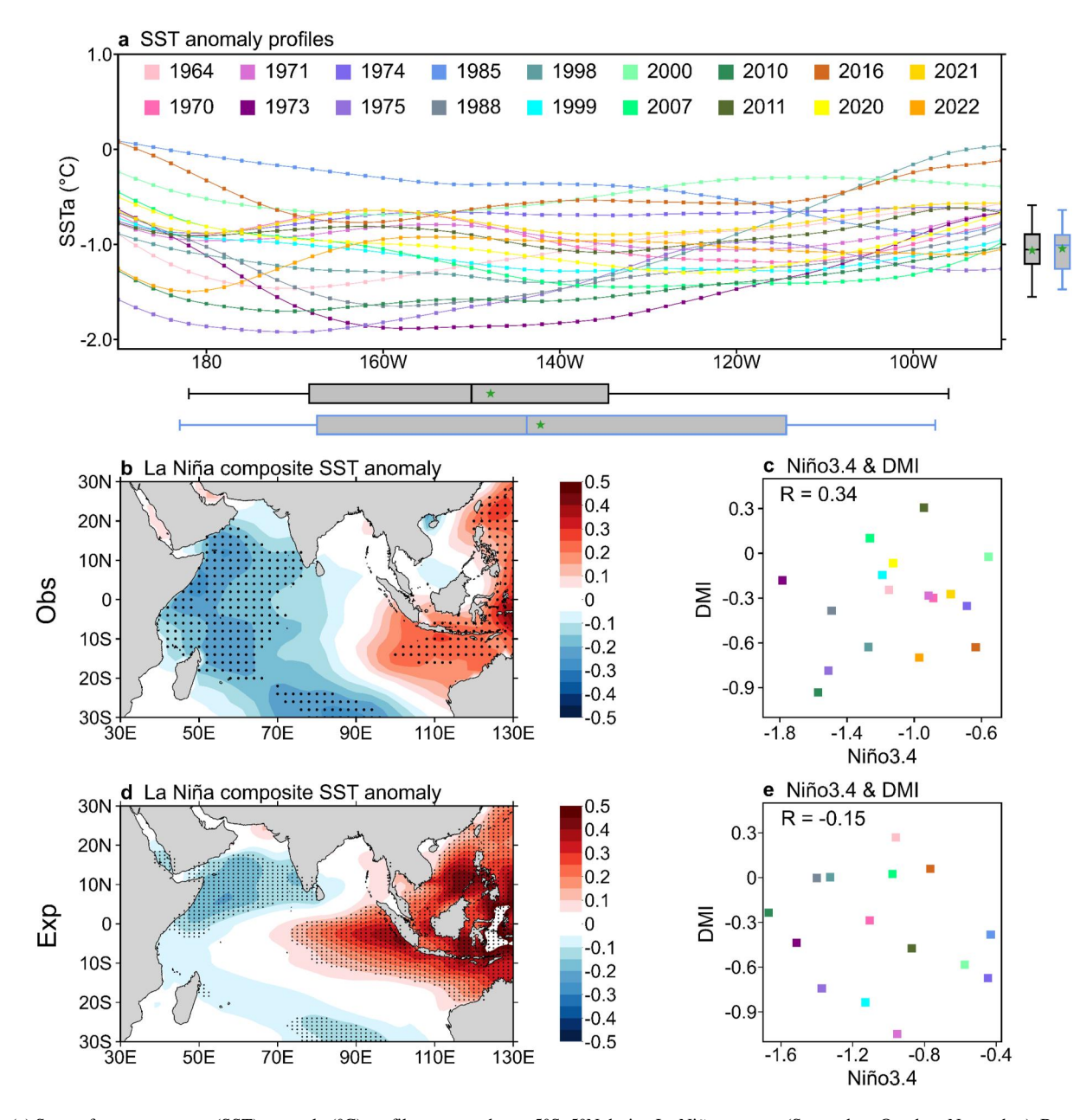


Figure 1. (a) Sea surface temperature (SST) anomaly (°C) profiles averaged over 5°S–5°N during La Niña autumns (September–October–November). Box and whisker plots (black for observation and blue for experiment) for the distribution of intensity (vertical) and zonal location (horizontal) of La Niña. Boxes extend from 25th to 75th percentile and whiskers range from minimum to maximum values. Green star and line in the box indicate the mean and median value, respectively. Longitudinal position of La Niña is defined as the longitude with the minimum value of SST anomalies averaged over 5°S–5°N. (b) Composite of SST anomalies during La Niña autumns. Black dots indicate SST anomalies that are statistically significant at the 0.05 significance level. (c) Scatterplot of the autumn Niño3.4 index against the simultaneous DMI during La Niña events. Correlation coefficient is shown in the upper left corner. (d, e) The same as (b, c) but for the pacemaker experiments.

fluxes. The constant ρ corresponds to the density of water (=10³ kg m⁻³), and c_p represents the specific heat of water (=4,000 J kg⁻¹ K⁻¹). The parameter H denotes the mixed layer depth, and R indicates the residual term in the equation.

3. Results

3.1. Connection Between La Niña SST Anomaly Longitudinal Position and IOD

First, Figure 1b shows the composited SST anomaly pattern in the tropical IO during La Niña autumn (September–October–November). Typically, La Niña events are accompanied by negative IOD-related SST

ZHANG ET AL. 3 of 10

anomalies in the tropical IO, manifesting negative SST anomalies in the tropical western IO and positive SST anomalies along the Java-Sumatra coast, consistent with previous studies (e.g., Baquero-Bernal et al., 2002). However, we can observe a moderate correlation between the intensity of IOD and that of La Niña (r = 0.34, insignificant at the 0.05 significance level) (Figure 1c). We extend our analysis to the pacemaker experiment (Figures 1d and 1e), yielding a similar conclusion that the La Niña amplitude is not a key factor in regulating its relationship with the IOD. It suggests that a stronger La Niña event does not necessarily lead to a significantly stronger negative IOD event. This intricate linkage introduces challenges for the seasonal prediction of the IOD, even when the SST anomaly amplitude in the tropical Pacific is precisely anticipated.

As shown in Figure 1a, La Niña shows large diversity in its longitudinal position during autumn. On average, the La Niña SST anomalies tend to peak in the central Pacific near 150°W, as evident from the mean and median value in the box plot. The zonal extent of the SST anomaly center during La Niña events ranges roughly from 180° E in the west to 100°W in the east. For instance, the recent triple-dip La Niña events spanning 2020–2022 displayed notably distinct zonal SST anomaly structures during three consecutive autumns. In autumn 2020 and 2021, the SST anomaly centers were situated near 125°W and 135°W respectively, whereas in autumn 2022, a conspicuous westward displacement was observed toward 180°E. These 3 years witnessed distinct SST anomalies across the tropical IO. Intriguingly, during the westmost La Niña of 2022, the corresponding IOD was significantly stronger compared to the other two years. We further examine the relationship of the IOD with the longitudinal position of La Niña-related SST anomalies. As shown in Figure 2a, there is a significant correlation between the intensity of IOD and the longitudinal position of La Niña (r = 0.63, significant at the 0.05 significance level). Here the longitudinal position of La Niña is defined as the longitude of the maximum negative SST anomalies in the equatorial Pacific averaged at 5°S-5°N. The westward-displaced La Niña events tend to accompany the stronger IOD events, while the eastward-displaced La Niña events correspond to the weak IOD conditions. Based on the linear fitting (Figure 2a), we are able to offer a rough estimation of the threshold of La Niña's zonal location (\sim 140°W) for a significant IOD (defined as a deviation below -0.5 standard deviation).

The positive relationship is also evident in the 10-member ensemble mean of targeted pacemaker experiments. These pacemaker experiments exclusively prescribed observed tropical Pacific forcing, enabling the rest of the coupled climate system to evolve independently. The simulations employing the nudge scheme (https://www.cesm.ucar.edu/working-groups/climate/simulations/cesm2-pacific-pacemaker) can realistically reproduce the Pacific SST conditions, although not in exact consistency with observations (Figure S1 in Supporting Information S1). Consequently, the ensemble mean of the simulated equatorial IO variability can serve as an approximation of the ENSO-driven IOD variability. We extend our investigation by using longer-term observation during 1880–2022 and pacemaker experiments during 1880–2019 and the qualitative result of the relationship between La Niña and IOD remains unchanged (Figure S2 in Supporting Information S1).

The remarkable consistency of the relationship of IOD with the La Niña longitudinal location between the experiments and observation underscores the prominent influence of the remote ENSO effects on the year-to-year IOD variability (Figures 2a and 2b). The key role of the zonal location of La Niña in the IOD variability is basically independent of that of the La Niña amplitude in a linear view. As shown in Figures 2c and 2d, no significant relationship between the La Niña amplitude and longitudinal location can be detected in the observation and pacemaker experiments. Previous studies have shown that the ENSO's intensity can be characterized by considering the varying ENSO's longitudinal location (Xie et al., 2020; Zhang et al., 2019). We also measured La Niña's intensity as the average SST anomalies extending from 25° west to 25° east of its longitudinal position. Using this definition, the qualitative conclusion remains the same. It needs to be clarified that we are not suggesting that the La Niña's intensity plays no role in its teleconnection to the IOD. The difference in correlation coefficients of IOD with the zonal location and intensity of La Niña is significant in the pacemaker experiments; however, it is not the case in the observation. It suggests that La Niña's intensity could also play some role in its connection with the IOD (Figure S3a in Supporting Information S1). We also examined the difference in correlation coefficients of IOD with the zonal location and intensity of La Niña in the output of the pi-control simulations from 47 CMIP6 climate models. The observed relationship between La Niña and IOD appears blurred in the majority of models (Figure S4 in Supporting Information S1), potentially attributed to bias in simulating a background equatorial Pacific cold tongue (e.g., Davey et al., 2002). In addition, in Figure 2b, we display the uncertainty of the IOD variability among the 10 members, which shows that the internal variability in the tropical IO cannot be neglected, consistent with the previous studies (Cai et al., 2009; Saji & Yamagata, 2003; Wang et al., 2023; Yamagata et al., 2004; Zhang et al., 2018).

ZHANG ET AL. 4 of 10

19448007, 2024, 3, Downloaded from https://agupubs.onlinelibrary.wiley.com/doi/10.1029/2023GL107119, Wiley Online Library on [18/04/2024]. See the Terms and Conditions (https://onlinelibrary.wiley.com/terms-and-conditions) on Wiley Online Library for rules of use; OA articles are governed by the applicable Creative Commons Licenses

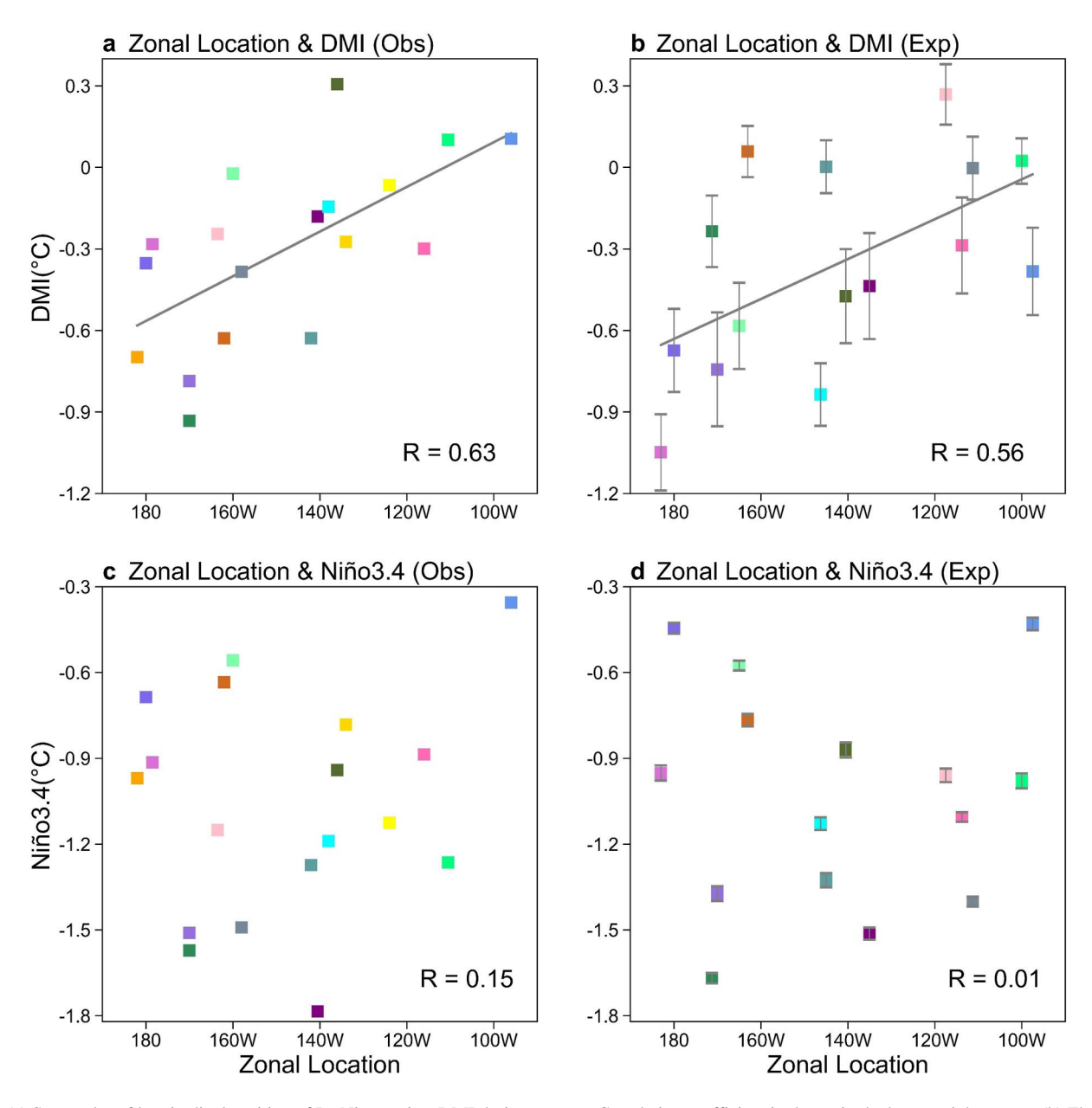


Figure 2. (a) Scatterplot of longitudinal position of La Niña against DMI during autumn. Correlation coefficient is shown in the bottom right corner. (b) The same as (a) but for pacemaker experiments. The linear fits (gray line) in (a, b) are displayed together with the correlation coefficients R. (c) Scatterplot of longitudinal position of La Niña against and its amplitude described as Niño3.4 index. (d) The same as (c) but for pacemaker experiments. The error bars for the ensemble mean in (b, d) correspond to 0.5 standard deviations.

3.2. Physical Mechanism for Impact of La Niña With Different Longitudinal Positions on IOD

As demonstrated in Section 3.1, La Niña's teleconnection to the IOD is largely associated with its longitudinal position of SST anomalies, rather than its intensity. Here, we employ a composite analysis to investigate potential physical mechanisms driving this La Niña-IOD relationship. Based on the SST anomaly longitudinal location of La Niña, we choose six westmost La Niña events (1971, 1974, 1975, 2000, 2010, 2016) and five eastmost La Niña events (1970, 1985, 1999, 2007, 2011). The west group of La Niña events is averagely located around 170°W, approximately 30 degrees of longitude farther westward compared to the east group (Figures 3a and 3b). These two La Niña groups exhibit a comparable intensity in SST anomaly center (Figure S5 in Supporting Information S1), suggesting that the intensity might play a minor role in driving the differences in their atmospheric responses. For the westward-displaced La Niña events, we observe significant convection suppression in the

ZHANG ET AL. 5 of 10

19448007, 2024, 3, Downloaded from https://agupubs.onlinelibrary.wiley.com/doi/10.1029/2023GL107119, Wiley Online Library on [18/04/2024]. See the Terms and Conditions (https://onlinelibrary.wiley.com/terms/

and-conditions) on Wiley Online Library for rules of use; OA articles are governed by the applicable Creative Commons License.

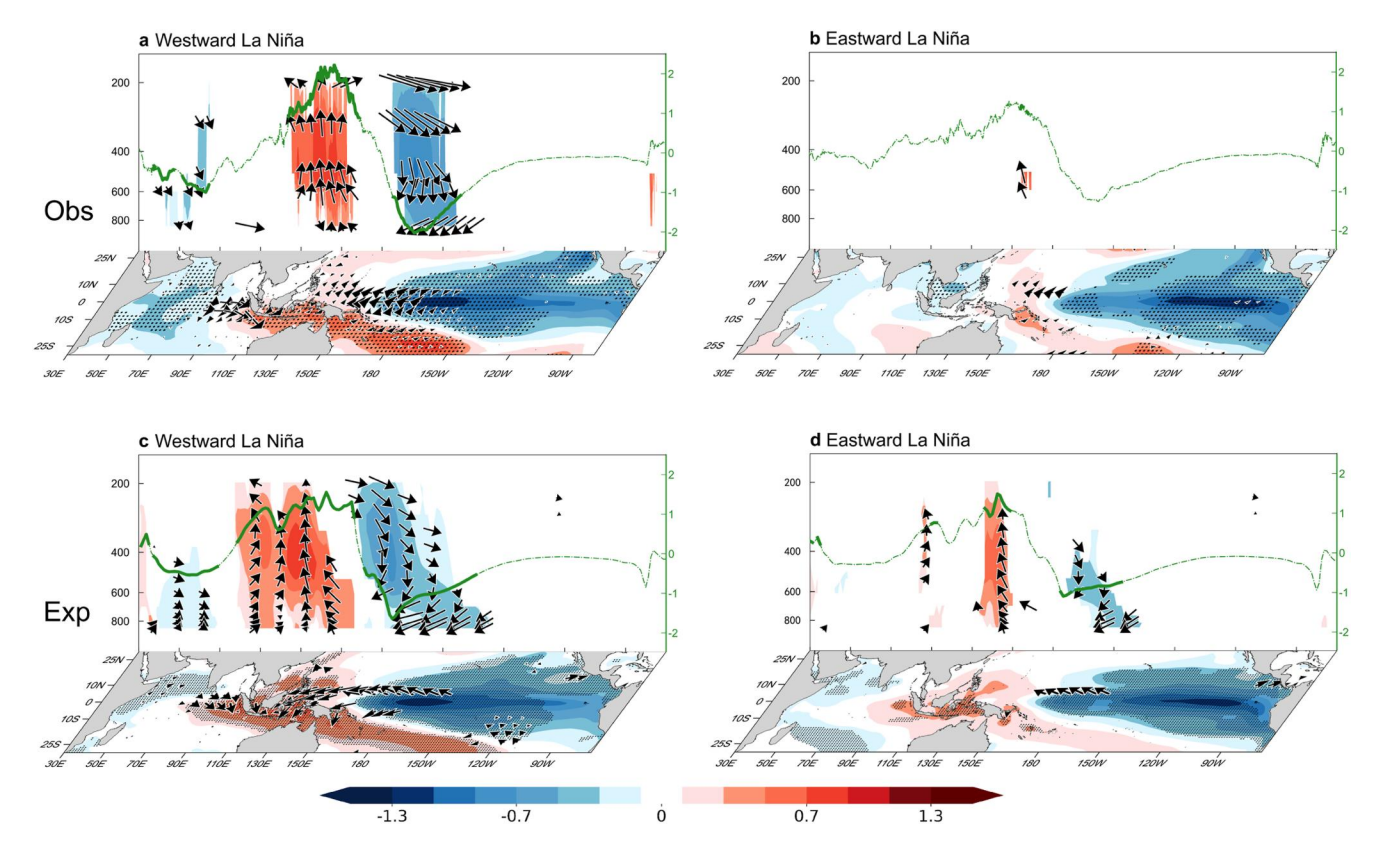


Figure 3. (a) Composites of zonal wind and vertical pressure velocity (vector; m/s) and precipitation anomalies (green; mm/day) averaged over 5° S– 5° N, and sea surface temperature anomalies (shading; $^{\circ}$ C) and surface wind anomalies (vector; m/s) for westward-displaced La Niña events. The vertical velocity anomalies are multiplied by a factor of -100 for the vectors and multiplied by a factor of -30 shown in shading (only shown when vertical velocity anomalies are significant at the 0.05 significance level). Dots and bold profiles indicate the composites that are statistically significant at the 0.05 significance level. (b) The same as (a) but for eastward-displaced La Niña events. (c, d) The same as (a, b) but for pacemaker experiments.

central Pacific and remarkable enhancement in the western Pacific (Figure 3a). Concurrently, the Walker Circulation in the Indo-Pacific region strengthens, characterized by anomalous descending motion near the dateline and anomalous ascending motion over the western Pacific. Accompanied by the anomalous ascending motion, a robust anomalous convergence occurs over the Indo-Pacific region in the lower troposphere. Surface westerly anomalies can effectively transport the warm water eastward along the equatorial IO, facilitating the occurrence of warm water in the eastern IO (Figure 4a). The tropical IO SST anomalies can further enhance the surface westerly anomalies through a positive Bjerknes feedback loop, fostering the IOD's development and maintenance. In comparison, the east group of La Niña shows a weak atmospheric response over the tropical Pacific (Figure 3b). Consequently, we find much weaker ascending motion over the western Pacific and an absence of significant westerly anomalies over the tropical IO, which are insufficient to initiate the negative IOD event. We can also classify the La Niña events based on the intensity of IOD, and similarly a stronger negative IOD event tends to correspond with a westward-displaced La Niña event (Figures S6a and S6c in Supporting Information S1). Similar conclusion can be drawn in the pacemaker experiments with the tropical Pacific SST forcing (Figures 3c and 3d; Figures S6b and S6d in Supporting Information S1), again confirming the importance of the La Niña longitudinal position in its impact on the IOD development.

The subsequent scientific question that requires understanding is the mechanism responsible for the substantial variation in IOD variability among La Niña events with distinct longitudinal locations. The La Niña's teleconnection to the IOD is closely linked to the initiation of the local convection. It has been shown in previous studies that convection anomalies in the tropics exhibit a nonlinear relationship with the underlying SST, with a convection threshold near 27.5°C (Gadgil et al., 1984; Graham & Barnett, 1987). That being said, the convection is sensitive to the SST change when the total SST remains above the threshold, whereas a weak response appears when the SST falls below it. For the westward-displaced La Niña events, the relatively strong negative SST

ZHANG ET AL. 6 of 10

1944807, 2024, 3, Downloaded from https://agupubs.onlinelibrary.wiley.com/doi/10.1029/2023GL107119, Wiley Online Library on [18/04/2024]. See the Terms and Conditions (https://onlinelibrary.wiley.com/terms-and-conditions) on Wiley Online Library for rules of use; OA articles are governed by the applicable Creative Commons License

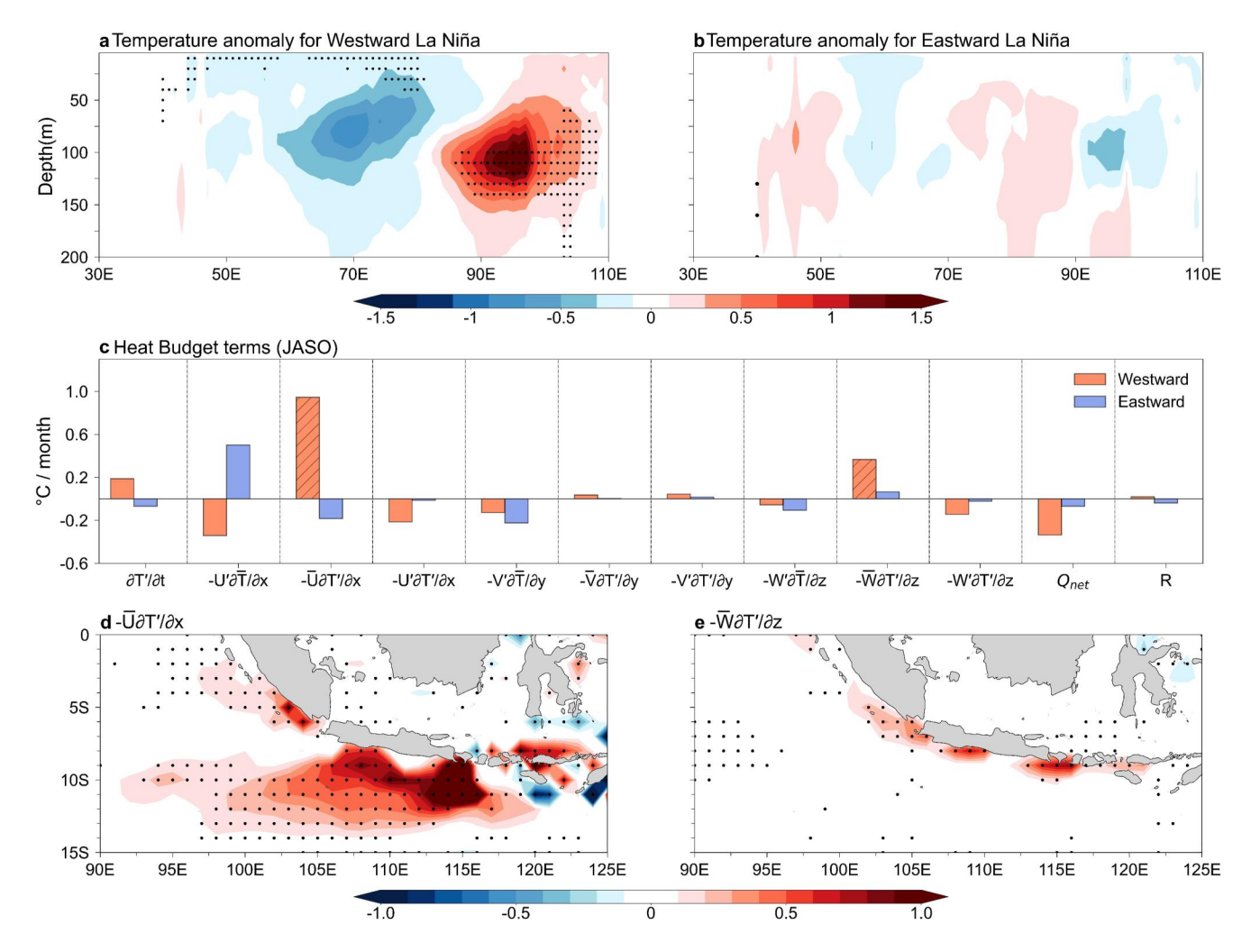


Figure 4. (a) Composite of upper 200m temperature anomalies (°C) averaged over 10° S to 10° N for westward-displaced La Nña events. (b) The same as (a) but for eastward-displaced La Nña events. (c) Heat budget terms averaged over the eastern tropical IO $(10^{\circ}\text{S}-0^{\circ})$ and $105^{\circ}\text{E}-125^{\circ}\text{E}$). Slash indicates the values that are statistically significant at the 0.05 significance level. (d, e) Difference in the two main terms $(-\overline{U}\partial T'/\partial x', -\overline{W}\partial T'/\partial z')$ in (c) between the westward-displaced and eastward-displaced La Nña events. Dots indicate the anomalies that are statistically significant at the 0.05 significance level.

anomalies extend into the central Pacific, where the background SSTs surpass the convection threshold (Figure 3a). Therefore, the convection is significantly inhibited in the central Pacific. When the La Niña-related SST anomaly center shifts to the eastern equatorial Pacific, it cannot effectively initiate convection anomalies considering that the background SSTs in the cold tongue region are already below the convection threshold (Figure 3b).

We extend our investigation through a heat budget analysis of SST anomalies within the tropical IO region. Here, the analyses are conducted in the July–August–September–October (leading the IOD mature phase by about 2 months) to detect dynamical and thermodynamical contributions shaping the IOD development. Here, our focus is on the eastern tropical IO for the heat budget analysis, since the SST difference emerges mainly in the eastern tropical IO between the westward-displaced and eastward-displaced La Niña events (Figure S7 in Supporting Information S1). Following the previous study (Du et al., 2005), we adopt a mixed layer depth of 40 m. In the eastern IO, two dominant terms linked to the IOD development (i.e., zonal advection and thermocline feedback) exhibit obvious differences. In general, the contribution of zonal advection term is larger than that of thermocline feedback term. For the westward-displaced La Niña events, these two terms are notably significant and robust (Figures 4c and 4d), whereas for the eastward-displaced ones, they are considerably weak (Figure 4c). The difference in the zonal advection term between the westward-displaced and eastward-displaced La Niña events is

ZHANG ET AL. 7 of 10

19448007, 2024, 3, Downloaded from https://agupubs.onlinelibrary.wiley

.com/doi/10.1029/2023GL107119, Wiley Online Library on [18/04/2024]. See the Terms

pronounced, covering most part of the southeastern tropical IO (Figure 4d). In contrast, the difference in the thermocline feedback term is relatively weak and is confined in the region along the Java-Sumatra coast.

4. Conclusions and Discussion

The present study investigates the complicated connection between La Niña and IOD and finds that the La Niña's teleconnection to the IOD is significantly associated with its longitudinal position both in the observation and the pacemaker experiments. For the westward-displaced La Niña events, the negative SST anomaly center is located in the central Pacific, near the eastern edge of the Pacific warm pool, which produces significant convection depression. The corresponding enhanced Walker Circulation is accompanied by the westerly wind anomalies in the tropical IO, thereby facilitating the negative IOD development. For the eastward-displaced La Niña events, the negative SST anomalies are primarily shifted to the eastern Pacific into the Pacific cold tongue region. Owing to the nonlinear relationship between SST and convection, these negative SST anomalies fail to trigger remarkable convection anomalies as the background SST falls below the convection threshold. Consequently, the eastward-displaced La Niña events bring about weak change in the Walker Circulation and thus no significant SST anomalies in the tropical IO.

It is noted that the ENSO exhibits pronounced asymmetry in its impact on the IOD. Our previous study has shown that the different flavors of El Niño (i.e., EP and CP El Niño) exhibit distinct relationships with the IOD (Zhang, Wang, Jin, et al., 2015; Zhang, Wang, Xiang, et al., 2015). In contrast, the observed La Niña's teleconnection to the IOD is mainly linked to its longitudinal position. The intensity of the eastward-displaced La Niña events has no significant correlation with the IOD amplitude, unlike the eastward-displaced El Niño events that show a high correlation between its intensity and that of IOD. This discrepancy can be comprehended by the nonlinear SST-convection relationship in the tropics. Positive SST anomalies superimposed on a background cold tongue SST can potentially lead to obvious convection changes when the total SST is above the convection threshold. However, negative SST anomalies result in feeble convection response due to the excessively cold conditions in the cold tongue. The complicated relationship between ENSO and IOD makes it challenging to achieve a skillful seasonal prediction in the tropical Indian Ocean region by utilizing the tropical Pacific information. How to translate the identified physical linkages between climate modes into operational forecast skill deserves future investigation.

Data Availability Statement

The global SST analysis from the Extended Reconstructed SST V5 data set (ERSST V5) provided by the National Oceanic and Atmospheric Administration (NOAA) at https://psl.noaa.gov/data/gridded/data.noaa.ersst.v5.html (Huang et al., 2017) is used in this study. Horizontal wind, vertical velocity and precipitation are derived from the fifth major global reanalysis produced by the European Centre for Medium-Range Weather Forecasts (ECMWF) (ERA5; Hersbach et al., 2023a, 2023b). The ocean temperature and horizontal currents and net downward heat flux ($Q_{\rm net}$) were investigated by using the ECMWF Ocean Reanalysis System 5 (ORAS5) (Copernicus Climate Change Service, Climate Data Store, 2021). In subsurface ocean, the geometric vertical velocity is employed based on National Centers for Environmental Prediction (NCEP) Global Ocean Data Assimilation System (GODAS) (https://www.psl.noaa.gov/data/gridded/data.godas.html) (Behringer et al., 1998). To evidence the main conclusion based on the observation, we further examined the outputs from ensembles of tropical Pacific Pacemaker experiments (comprising 10 members) using the National Center for Atmospheric Research Community Earth System Model version 2 (NCAR CESM2) (Nan et al., 2022). The CMIP6 model data sets are available at the Earth System Grid Federation (ESGF) at https://esgf-node.llnl.gov/search/cmip6/.

Acknowledgments

This work was supported by the National Key R&D Program of China (2022YFF0801602) and the National Nature Science Foundation of China (42088101).

References

Alexander, M. A., Bladé, I., Newman, M., Lanzante, J. R., Lau, N. C., & Scott, J. D. (2002). The atmospheric bridge: The influence of ENSO teleconnections on air-sea interaction over the global oceans. *Journal of Climate*, 15(16), 2205–2231. https://doi.org/10.1175/1520-0442(2002) 015<2205:TABTIO>2.0.CO;2

Allan, R. J., Chambers, D., Drosdowsky, W., Hendon, H., Latif, M., Nicholls, N., et al. (2001). Is there an Indian Ocean Dipole independent of the El Niño–Southern Oscillations? *CLIVAR Exch*, 6(3), 18–22.

Annamalai, H., Murtugudde, R., Potemra, J., Xie, S. P., Liu, P., & Wang, B. (2003). Coupled dynamics over the Indian Ocean: Spring initiation of the zonal mode. *Deep-Sea Research*, 50(12–13), 2305–2330. https://doi.org/10.1016/s0967-0645(03)00058-4

Ashok, K., Behera, S. K., Rao, S. A., Weng, H., & Yamagata, T. (2007). El Niño Modoki and its possible teleconnection. *Journal of Geophysical Research*, 112(C11), C11007. https://doi.org/10.1029/2006JC003798

ZHANG ET AL. 8 of 10

- Ashok, K., Guan, Z., & Yamagata, T. (2001). Impact of the Indian Ocean dipole on the relationship between the Indian monsoon rainfall and ENSO. *Geophysical Research Letters*, 28(23), 4499–4502. https://doi.org/10.1029/2001GL013294
- Baquero-Bernal, A., Latif, M., & Legutke, S. (2002). On dipolelike variability of sea surface temperature in the tropical Indian Ocean. *Journal of Climate*, 15(11), 1358–1368. https://doi.org/10.1175/1520-0442(2002)015<1358:ODVOSS>2.0.CO;2
- Behringer, D. W., Ji, M., & Leetmaa, A. (1998). An improved coupled model for ENSO prediction and implications for ocean initialization. Part I: The ocean data assimilation system. *Monthly Weather Review*, 126(4), 1013–1021. https://doi.org/10.1175/1520-0493(1998)126<1013: aicmfe>2.0 co:2
- Cai, W., & Cowan, T. (2008). Dynamics of late autumn rainfall reduction over southeastern Australia. Geophysical Research Letters, 35(9), L09708. https://doi.org/10.1029/2008GL033727
- Cai, W., & Cowan, T. (2009). La Niña Modoki impacts Australia autumn rainfall variability. Geophysical Research Letters, 36(12), L12805. https://doi.org/10.1029/2009GL03788
- Cai, W., Pan, A., Roemmich, D., Cowan, T., & Guo, X. (2009). Argo profiles a rare occurrence of three consecutive positive Indian Ocean Dipole events, 2006-2008. Geophysical Research Letters, 36(8). https://doi.org/10.1029/2008gl037038
- Copernicus Climate Change Service, Climate Data Store. (2021). ORAS5 global ocean reanalysis monthly data from 1958 to present [Dataset]. Copernicus Climate Change Service (C3S) Climate Data Store (CDS). https://doi.org/10.24381/cds.67e8eeb7
- Danabasoglu, G., Lamarque, J.-F., Bacmeister, J., Bailey, D. A., DuVivier, A. K., Edwards, J., et al. (2020). The Community Earth System Model Version 2 (CESM2). Journal of Advances in Modeling Earth Systems, 12(2), e2019MS001916. https://doi.org/10.1029/2019MS001916
- Davey, M. K., Huddleston, M., Sperber, K. R., Braconnot, P., Bryan, F. O., Chen, D., et al. (2002). STOIC: A study of coupled model climatology and variability in tropical ocean regions. Climate Dynamics, 18(5), 403–420. https://doi.org/10.1007/s00382-001-0188-6
- Du, Y., Qu, T., Meyers, G., Masumoto, Y., & Sasaki, H. (2005). Seasonal heat budget in the mixed layer of the southeastern tropical Indian Ocean in a high-resolution ocean general circulation model. *Journal of Geophysical Research*, 110(C4), C04012. https://doi.org/10.1029/2004JC002845
- Fan, L., Liu, Q., Wang, C., & Guo, F. (2017). Indian Ocean dipole modes associated with different types of ENSO development. *Journal of Climate*, 30(6), 2233–2249. https://doi.org/10.1175/JCLI-D-16-0426.1
- Gadgil, S., Joseph, P., & Joshi, N. (1984). Ocean–atmosphere coupling over monsoon regions. *Nature*, 312(5990), 141–143. https://doi.org/10.1038/312141a0
- Graham, N. E., & Barnett, T. P. (1987). Sea surface temperature, surface wind divergence, and convection over tropical oceans. *Science*, 238/4827, 657, 659, https://doi.org/10.1126/science.238/4827.657
- 238(4827), 657–659. https://doi.org/10.1126/science.238.4827.657
 Hersbach, H., Bell, B., Berrisford, P., Biavati, G., Horányi, A., Muñoz Sabater, J., et al. (2023a). ERA5 monthly averaged data on pressure levels
- from 1940 to present [Dataset]. Copernicus Climate Change Service (C3S) Climate Data Store (CDS). https://doi.org/10.24381/cds.6860a573
 Hersbach, H., Bell, B., Berrisford, P., Biavati, G., Horányi, A., Muñoz Sabater, J., et al. (2023b). ERA5 monthly averaged data on single levels
- from 1940 to present [Dataset]. Copernicus Climate Change Service (C3S) Climate Data Store (CDS). https://doi.org/10.24381/cds.f17050d7 Huang, B., Thorne, P. W., Banzon, V. F., Boyer, T., Chepurin, G., Lawrimore, J. H., et al. (2017). NOAA extended reconstructed sea surface temperature (ERSST), version 5 [Dataset]. NOAA National Centers for Environmental Information. https://doi.org/10.7289/V5T72FNM
- Jin, F., An, S., Timmermann, A., & Zhao, J. (2003). Strong El Niño events and nonlinear dynamical heating. *Geophysical Research Letters*, 30(3), 1120. https://doi.org/10.1029/2002GL016356
- Kao, H. Y., & Yu, J. Y. (2009). Contrasting eastern-Pacific and central-Pacific types of ENSO. *Journal of Climate*, 22(3), 615–632. https://doi.org/10.1175/2008ICL12309.1
- Klein, S. A., Soden, B. J., & Lau, N.-C. (1999). Remote sea surface temperature variations during ENSO: Evidence for a tropical atmospheric bridge. *Journal of Climate*, 12(4), 917–932. https://doi.org/10.1175/1520-0442(1999)012<0917:RSSTVD>2.0.CO;2
- Kug, J. S., & Ham, Y. G. (2011). Are there two types of La Niña? Geophysical Research Letters, 38(16), L16704. https://doi.org/10.1029/
- Kug, J.-S., Jin, F.-F., & An, S.-I. (2009). Two types of El Niño events: Cold tongue El Niño and warm pool El Niño. Journal of Climate, 22(6), 1499–1515. https://doi.org/10.1175/2008JCLI2624.1
- Larkin, N. K., & Harrison, D. E. (2005). Global seasonal temperature and precipitation anomalies during El Niño autumn and winter. *Geophysical Research Letters*, 32(16), L16705. https://doi.org/10.1029/2005GL022860
- Lau, N.-C., & Nath, M. J. (2003). Atmosphere–ocean variations in the Indo-Pacific sector during ENSO episodes. *Journal of Climate*, 16(1), 3–20. https://doi.org/10.1175/1520-0442(2003)016<0003; AOVITI>2.0.CO:2
- Li, T., Wang, B., Chang, C.-P., & Zhang, Y. (2003). A theory for the Indian ocean dipole-zonal mode. *Journal of the Atmospheric Sciences*, 60(17), 2119–2135. https://doi.org/10.1175/1520-0469(2003)060<2119:ATFTIO>2.0.CO;2
- Liu, M., McPhaden, M. J., Ren, H.-L., Balmaseda, M. A., & Wang, R. (2022). Oceanic heat content as a predictor of the Indian Ocean Dipole. Journal of Geophysical Research: Oceans, 127(12), e2022JC018896. https://doi.org/10.1029/2022JC018896
- Nan, R., Simpson, I., & Adam, P. (2022). CESM2 Pacific pacemaker ensemble [Dataset]. UCAR/NCAR Climate and Global Dynamics Laboratory. https://doi.org/10.26024/gtrs-tf57
- Ren, H. L., & Jin, F. F. (2011). Niño indices for two types of ENSO. Geophysical Research Letters, 38(4), L04704. https://doi.org/10.1029/2010GL046031
- Saji, N. H., Goswami, B. N., Vinayachandran, P. N., & Yamagata, T. (1999). A dipole in the tropical Indian Ocean. *Nature*, 401(6751), 360–363. https://doi.org/10.1038/43854
- Saji, N. H., & Yamagata, T. (2003). Structure of SST and surface wind variability during Indian Ocean Dipole mode events: COADS observations. Journal of Climate, 16, 2735–2751. https://doi.org/10.1175/1520-0442(2003)016<2735:SOSASW>2.0.CO;2
- Scott, A. F., Xiang, S.-P., & McCreary, J. P., Jr. (2009). Indian Ocean circulation and climate variability. Reviews of Geophysics, 47(1), RG1002. https://doi.org/10.1029/2007RG000245
- Stuecker, M. F., Timmermann, A., Jin, F.-F., Chikamoto, Y., Zhang, W., Wittenberg, A. T., et al. (2017). Revisiting ENSO/Indian Ocean Dipole phase relationships. *Geophysical Research Letters*, 44(5), 2481–2492. https://doi.org/10.1002/2016GL072308
- Wang, H., Kumar, A., Murtugudde, R., Narapusetty, B., & Seip, K. L. (2019). Covariations between the Indian Ocean Dipole and ENSO: A modeling study. Climate Dynamics, 53(9–10), 5743–5761. https://doi.org/10.1007/s00382-019-04895-x
- Wang, J., Zhang, S., Jiang, H., & Yuan, D. (2023). Effects of 2019 subsurface Indian Ocean initialization on the forecast of the 2020/2021 La Niña event. Climate Dynamics, 60(7), 2419–2435. https://doi.org/10.1007/s00382-022-06442-7
- Webster, P. J., Moore, A. M., Loschnigg, J. P., & Leben, R. R. (1999). Coupled oceanic-atmospheric dynamics in the Indian Ocean during 1997–98. Nature, 401(6751), 356–360. https://doi.org/10.1038/43848
- Xie, R., Mu, M., & Fang, X. (2020). New indices for better understanding ENSO by incorporating convection sensitivity to Sea Surface temperature. *Journal of Climate*, 33(16), 7045–7061. https://doi.org/10.1175/JCLI-D-19-0239.1

ZHANG ET AL. 9 of 10

Geophysical Research Letters

- 10.1029/2023GL107119
- Xie, S.-P., Annamalai, H., Schott, F. A., & McCreary, J. P. (2002). Structure and mechanisms of south Indian Ocean climate variability. *Journal of Climate*, 15(8), 867–878. https://doi.org/10.1175/1520-0442(2002)015<0864;SAMOSI>2.0.CO;2
- Yamagata, T., Behera, S. K., Luo, J. J., Masson, S., Jury, M. R., & Rao, S. A. (2004). Coupled ocean-atmosphere variability in the tropical Indian Ocean. *Earth's Climate*, 147, 189–212. https://doi.org/10.1029/147GM12
- Zhang, L., Du, Y., & Cai, W. (2018). Low-frequency variability and the unusual Indian Ocean Dipole events in 2015 and 2016. Geophysical Research Letters, 45(2), 1040–1048. https://doi.org/10.1002/2017gl076003
- Zhang, W., Wang, L., Xiang, B., Qi, L., & He, J. (2015). Impacts of two types of La Niña on the NAO during boreal winter. Climate Dynamics, 44(5–6), 1351–1366. https://doi.org/10.1007/s00382-014-2155-z
- Zhang, W., Wang, Y., Jin, F.-F., Stuecker, M. F., & Turner, A. G. (2015). Impact of different El Niño types on the El Niño/IOD relationship. Geophysical Research Letters, 42(20), 8570–8857. https://doi.org/10.1007/s00382-018-4135-1
- Zhang, W. J., Mao, W., Jiang, F., Stuecker, M. F., Jin, F. F., & Qi, L. (2021). Tropical Indo-Pacific compounding thermal conditions drive the 2019 Australian extreme drought. *Geophysical Research Letters*, 48(2), e2020GL090323. https://doi.org/10.1029/2020GL090323
- Zhang, Z., Ren, B., & Zheng, J. (2019). A unified complex index to characterize two types of ENSO simultaneously. *Scientific Reports*, 9(1), 8373. https://doi.org/10.1038/s41598-019-44617-1
- Zhao, S., Stuecker, M. F., Jin, F.-F., Feng, J., Ren, H.-L., Zhang, W., & Li, J. (2020). Improved predictability of the Indian Ocean Dipole using a stochastic dynamical model compared to the North American multimodel ensemble forecast. Weather and Forecasting, 35(2), 379–399. https://doi.org/10.1175/WAF-D-19-0184.1

ZHANG ET AL. 10 of 10